Aerosol optical depth determination in the UV using a four-channel precision filter radiometer

Thomas Carlund[1,a], Natalia Kouremeti[1], Stelios Kazadzis[1], Julian Gröbner[1]

[1] Physikalisch-Meteorologisches Observatorium Davos/World Radiation Center (PMOD/WRC), Dorfstrasse 33, CH-7260 Davos Dorf, Switzerland

[a] From 1 April 2017 at Swedish Meteorological and Hydrological Institute, SE-60176 Norrköping, Sweden

Correspondence to: Thomas Carlund (thomas.carlund@pmodwrc.ch, thomas.carlund@smhi.se)

Abstract. The determination of aerosol properties, especially the aerosol optical depth (AOD) in the UV wavelength region is of great importance to understand the climatological variability of UV radiation. However, operational retrievals of AOD at the biological most harmful wavelengths in the UVB are currently only made at very few places. This paper reports on the UVPFR sunphotometer, a stable and robust instrument that can be used for AOD retrievals at four UV wavelengths. Instrument characteristics and results of Langley calibrations at a high altitude site were presented. It was shown that due to the relatively wide spectral response functions of the UVPFR, the calibration constants (V_0) from Langley plot calibrations underestimate the true extra-terrestrial signals. Accordingly, correction factors were introduced. In addition, the instrument spectral response functions also result in an apparent airmass dependent decrease in ozone optical depth used in the AOD determinations. An adjusted formula for the calculation of AOD, with a correction term dependent on total column ozone amount and ozone air mass, was therefore developed. Langley calibrations performed 13–14 months apart resulted in sensitivity changes of ≤1.1 %, indicating good instrument stability. Comparison with a standard PFR, measuring AOD at 368–862 nm wavelengths with high accuracy, showed consistent results. Also very good agreement was achieved comparing the UVPFR with AOD at UVB wavelengths derived with a Brewer spectrophotometer, which was calibrated against the UVPFR at an earlier date. Mainly due to non-instrumental uncertainties connected with ozone optical depth, the total uncertainty of AOD in the UVB are higher than the ones reported from UVA and visible AOD measuring instruments. However, the precision can be high between instruments using harmonized algorithms for ozone and Rayleigh optical depth as well as for air mass terms. For several months of comparison measurements with the UVPFR and a Brewer the root mean squared AOD differences were <0.01 at all the 306–320 nm Brewer wavelengths.

1 Introduction

Absorption and scattering of solar radiation by aerosols has been recognized as an important parameter for climate forcing studies (IPCC, 2013). Furthermore, the absorption of surface ultraviolet (UV) radiation by aerosols has also become of major interest because of the harmful effects of UV radiation on Humans and more generally on the biosphere (Madronich et al., 2015; UNEP, 2010). Especially in heavily polluted areas, the decrease of UVB radiation due to aerosol attenuation can

become larger than the expected increase of UV radiation due to the declining ozone levels (e.g. Zerefos et al., 2012; De Bock et al., 2014). Thus, the determination of aerosol properties, especially the aerosol optical depth (AOD) in the UV wavelength region is of great importance to understand the climatological variability of UV radiation.

The effect of aerosols on solar UV radiation is important as it is linked with the impact on UV radiation on human health,
5   atmospheric chemistry (e.g. Gerasopoulos et al., 2012) and the biosphere (Diffey, 1991). UV-B overexposure is related with various serious health damage effects such as skin cancer cataract, skin ageing, snow blindness and immune system changes (Rieder et al., 2008, Cordero et al., 2009). However, even if the aerosol attenuation on the solar UVB wavelength range is higher than the one at longer wavelengths, the most of available surface based and satellite AOD measurements are related with UVA and visible range.

10   Surface based instruments are currently providing AOD measurements at UVA wavelengths. The Aerosol Robotic Network (AERONET) (Holben et al., 1998) provides a number of instruments that are able to provide AOD at 340 nm and 380 nm, in addition, the Global Atmospheric Watch precision filter radiometer network (GAW-PFR) provides AOD at 368 nm (Wehrli, 2008). In order to extrapolate the UVA and visible AOD to the UVB the spectral dependence and the aerosol type is needed. This is because the simple Ångström power law includes a wavelength dependence that is related with the different aerosol
15   types, potentially leading to very poor accuracy of AOD in the UVB determined from extrapolation of accurate AOD values in the visible to near infrared range of the spectrum (Li et al., 2012).

Only limited instruments such as the UV multifilter radiometer (UVMFR) (Krotkov et al., 2005; Corr et al., 2009) could be used to provide AOD retrievals in the UVB wavelength range. The Brewer spectrophotometer is an instrument initially designed for providing total column ozone (*TCO*) measurements based on the use of direct sun measured irradiance at
20   specific wavelengths in the UVB range (e.g. Kerr et al., 1985). During the past years, several attempts have been presented in the literature, that showed the use of the above mentioned Brewer measurements in order to retrieve AOD in the UVB (e.g. Marenco et al., 1997; Marenco et al., 2002; Cheymol and De Backer, 2003; Cheymol et al., 2006; Gröbner and Meleti, 2004; Kazadzis et al. 2005; Kazadzis et al. 2007; Meleti et al., 2009; De Bock et al., 2010; Kumharn et al., 2012; De Bock et al., 2014). In addition, based on Brewer AOD retrievals, Arola and Koskela, 2004 have discussed the uncertainties and
25   possible systematic errors linked with the Brewer related direct sun retrieval for AOD.

Lately, the European COST project EUBREWNET, for harmonizing European Brewer spectrophotometer measurements, also aim at including an UVB aerosol optical depth product in the common data processing. In the course of this project PMOD/WRC has been working on a portable and stable instrument to be used for the intercalibration of the various Brewer instruments. As such, the UVPFR instrument built at PMOD/WRC has been used. Within this study we present the
30   characterization and calibration of the UVPFR instrument as well as validation through field measurements that have been performed at PMOD/WRC in Davos, Switzerland.

2 The UVPFR sunphotometer

2.1 Instrument development and characterization

The UVPFR sunphotometer is a special version of the Precision Filter Radiometer (PFR) designed and built in the late 1990s at the Physikalisch-Meteorologisches Observatorium Davos and World Radiation Center (PMOD/WRC) in Davos,

5 Switzerland. It measures the direct solar irradiance at the four nominal wavelengths 305, 311, 318 and 332 nm at bandwidths of approximately 1.0-1.3 nm at full width half maximum (FWHM). The detectors are operated in a controlled environment and are exposed to solar radiation only during actual measurements. A Peltier thermostat maintains the ion-assisted deposition filters and silicon detectors at a constant (±0.1°C) temperature of 20° C over an ambient temperature range from -20° C to +35° C. A shutter opens for only a few seconds during direct sun measurements to keep dose-related degradation of

10 the filters and detectors to a minimum. The vacuum tight sensor head is filled with dry nitrogen gas. In addition to the information given here, a more detailed description can be found in Ingold et al. (2001).

A recent improvement of the instrument was the addition of an UG11 low pass filter at all four channels to remove out of band leakage that had been observed in the original version of the UVPFR.

The spectral response functions of the UVPFR #1001 used in this study were measured in the laboratory at PMOD/WRC in

15 February 2016 and the resulting effective central wavelengths and FWHM are given in Table 1. The spectral response functions have also been convolved (spectral weighting taking into account each filter's spectral response function) with an extra-terrestrial solar spectrum and the results are given in column 3 of Table 1. These latter are the wavelengths used for calculating the Rayleigh optical depth for the UVPFR #1001. (The differences in Rayleigh optical depth for the two different sets of effective central wavelengths are <0.0007.) The latest measurements of the spectral response functions were also

20 compared with measurements that were performed in the initial stage of the instrument development, in 1999. The difference in effective central wavelengths was ≤0.05 nm at all four wavelengths. For the two shortest and therefore most sensitive wavelengths, the difference was only 0.02 nm. For the filter bandwidths, recent measurements have been used in order to improve their determination. In 2016 a tuneable EKSPLA NT 200 laser (www.ekspla.com) was used for the determination of the spectral response functions.

25 In order to perform direct sun measurements, the UVPFR is mounted on a sun-tracker so that it is continuously pointing to the Sun. The four photometric channels are measured simultaneously by a commercial data logger system (Campbell Scientific CR10X) with 13 bit resolution. Automatic signal ranging within the PFR and logger system is used to increase the dynamic range to 16 bits. The logger clock is frequently updated to be accurate within 1 second. Signal measurements made at full minutes are averages of 10 samples for each channel made over a total duration of 1.25 seconds and can be considered

30 as instantaneous values.

The full field of view of the instrument is 2.5° and the slope angle is 0.7°. An optical position sensor monitors the solar pointing within a ±0.5° range. Normally, the air pressure at station level is measured with a relative coarse accuracy (±1.0 hPa) barometer (Vaisala PTB101 or Setra Model 278) connected to the UVPFR logger box.

2.2 Instrument calibration

Calibration of reference sunphotometers with the Langley technique are preferably performed at high altitude stations since they require low and stable aerosol load (e.g. Shaw 1983). Difficulties with Langley calibrations at a low altitude and urban site, when calibration at a high altitude is not possible, has been discussed by Arola and Koskela (2004) and was recently

5 demonstrated by Diemoz et al. (2016). For instruments measuring at wavelengths affected by absorption in ozone, also stable total ozone amount is needed during the Langley related period of measurements. These requirements can be relatively frequently fulfilled at the Izaña Atmospheric Observatory (IZO) on the island of Tenerife (28.31° N, 16.50 °W) at an altitude of 2373 m. At IZO, the Izaña Atmospheric Research Centre (IARC) manages the Regional Brewer Calibration Center – Europe (RBCC-E) and it is the absolute sun calibration facility of PHOTONS and the Red Ibérica de medida Fotométrica de

10 Aeroseles (RIMA) networks. PHOTONS and RIMA are federated networks of the AERONET. In addition, IZO has been recognized as a WMO-CIMO testbed for aerosol remote sensing instruments including AERONET and GAW-PFR instrumentation.

During May to August 2015 the UVPFR #1001 was operated at the IZO station, with the exception of the time period from the 20 May to 10 June. In September 2016 the next Langley calibration at IZO was performed. In addition to the favourable

15 measurement conditions an advantage of the IZO station is the co-location of other instruments, such as Brewer spectrophotometers and standard PFR sunphotometers. These instruments measure among others total column ozone and AOD in the 368-862 nm range, respectively. These additional variables are highly valuable and help to determine whether measurement conditions during half days (mornings or afternoons) have been suitable for the so called Langley plot calibrations.

20 The classic Langley method to determine the calibration constant V_0 of each wavelength channel , being equal to the signal that would have been measured at the top of the atmosphere at mean Sun-Earth distance, has been described in many articles on sunphotometry (e.g. Shaw , 1983) and many variations thereof have been published over the last decades. The method is based on the inversion of the so-called Bouguer-Lambert-Beer's law, leading to

25 $$ln(V) = ln(V_0) - \delta m \tag{1}$$

where the wavelength dependent quantities $ln(V_0)$ and total optical depth δ can be determined by least-square methods from a number of cloud-free measurements of V taken at different air masses m. The calibration constant V_0 used to be found by linear extrapolation to zero air mass of measurements V plotted on a logarithmic scale versus air mass. This method is

30 historically called Langley plot calibration (Langley, 1903).

Using a single, common air mass m for all components of the total optical depth can lead to significant errors in $ln(V_0)$ (e.g. Thomason et al. 1983; Forgan, 1988; Russell et al., 1993; Schmid and Wehrli, 1995; Slusser et al. 2000). Two more accurate

variants of the Langley extrapolation used here replaces δm by the sum of components optical depth $\delta_R m_R + \delta_o m_o + \delta_a m_a$ and solves either of the equations

$$ln(R^2 V) + \delta_R m_R + \delta_o m_o = ln(V_0) - \delta_a m_a \qquad \text{or} \qquad (2)$$

$$ln(R^2 V) + \delta_R m_R = ln(V_0) - (\delta_o + \delta_a)m_{2ODw} \qquad (3)$$

for $ln(V_0)$ and aerosol optical depth (Eq. 2) or the sum of the two terms ozone and aerosol optical depth $(\delta_o + \delta_a)$ (Eq. 3). R is the actual Sun-Earth distance expressed in fraction to 1 AU. The airmass term m_{2ODw} is the ozone and aerosol optical depth

10   weighted sum of m_o and m_a., i.e. $m_{2ODw} = (\delta_o m_o + \delta_a m_a)/(\delta_o + \delta_a)$. The values on ozone and aerosol optical depth at IZO are in these cases calculated from total ozone measured by the RBCC-E Brewer spectrophotometer triad (GAW, 2015) and from the AOD measured by a standard PFR sunphotometer determining AOD at 368, 412, 500 and 862 nm and extrapolated to the actual UV wavelength using the Ångström relation. Langley calibrations based on equation 2, sometimes called refined Langley plots (Schmid and Wehrli, 1995), do not require any *a priori* AOD estimate and ozone changes are taken into

15   account if measured correctly. On the other hand, based on numerical tests, V_0 results using equation 3 were found less sensitive to errors in δ_o. For the Langley calibration of the UVPFR at the IZO station, very accurate measurements on both *TCO* and AOD(368-862nm) were available. As a result, the average V_0s at all UVPFR wavelengths differ 0.2 % or less between the two methods.

From the quality of the linear fit of the Langley plot and using *TCO* and AOD data from the other instruments, the selection

20   of exact airmass range (within 1.2–2.9), and validity of the Langley plot events was mainly based on subjective judging by the analyst. During the periods when the UVPFR #1001 was at IZO, 27 accepted Langley plot occasions were found in 2015 and 12 were found in 2016. The resulting V_0s from these events in 2015 for the method in Eq. (3) are shown in Fig. 1. In addition to the requirement of stable AOD, for the UVPFR it is important to have a stable ozone amount over the site. Or, when very accurate ozone measurements are available, as from the RBCC-E Brewer triad, small ozone changes during the

25   Langley plot periods can be accounted for. From the Brewer measurements the ozone change during each Langley event was calculated by fitting a linear function to the available *TCO* measurement data with respect to ozone airmass. The slope of the fit is the change in ozone per unit airmass. The final V_0s are then derived from interpolation to zero ozone change as shown in Fig. 1. From this figure it is also evident that the sensitivity to ozone change is low for the 332 nm channel. The sensitivity increases with decreasing wavelength. For the 305 nm channel there is more than 1 % change in V_0 per 1 DU

30   change per unit airmass during a Langley event. Similar results were found for the Langley plots in 2016.

In principle, *TCO* can also be estimated by the UVPFR itself. It is however believed that Brewer spectrophotometers are superior to the UVPFR in *TCO* determination. At the same time, it is important to remember that the Langley plot calibration of the UV-PFR becomes dependent on the ozone measurements when these are used to correct for ozone changes during

Langley events. In case there is a small airmass dependent error in the Brewer (triad) measurements, there will also be an error in the UVPFR V_0s.

As is clear from Fig. 1, taking just a single Langley plot event is not enough, if high accuracy accompanied with uncertainty estimation is aimed at. The (experimental) standard deviation of the V_0 of the refined method in 2015 is highest for the

5 shortest wavelength (1.28 %) and smallest for the longest wavelength (0.44 %). The standard deviation of the residuals to the linear fit of V_0s from equation 3 versus ozone change is 0.99 % at the shortest wavelength, and very close to the standard deviation of V_0 of the refined method at the other wavelengths. The standard deviations of the V_0s in 2016 were slightly lower than for the larger number of Langley plot results in 2015. In addition, the (experimental) standard deviation of the mean V_0 for both periods was 0.25 % and 0.23 %, respectively, for the shortest wavelength.

10 The final calibration values are shown in Table 2. Over the slightly more than a 1-year period between the calibrations at IZO, the decrease in sensitivity was as small as ≤0.2 % at the two shortest wavelength channels. For the 332 nm wavelength the change was -1.0 % and at the apparently least stable channel (318 nm) the change was -1.1 %. With only one channel just exceeding the goal stability of ≤1 % per year, the stability of the UVPFR #1001 is regarded as satisfactory.

2.3 Corrections due to the finite FWHM

15 Due to the large variation with wavelength in extra-terrestrial solar irradiance and ozone absorption in the UV, spectral transmission measurements need to be made at well-defined and narrow passbands in this wavelength region. The bandwidth of the UVPFR filters, in the order of 1nm, are significantly narrower than for standard VIS-NIR sunphotometers, but about twice as wide as the slit functions of Brewer spectrophotometers. Therefore, the effect of finite bandwidths was investigated for the UVPFR. Numbers on effective central wavelengths and full width at half maximum (FWHM) are given in Table 1.

20 Due to the strong exponential increase in ozone absorption with decreasing wavelength, and hence its stronger change with airmass at the shorter wavelength side of the filter band passes, this leads to an increase in the effective wavelengths seen by the UVPFR when the airmass increases. This in turn leads to errors in the extrapolation to zero airmass during a Langley calibration. The FWHM effect has been quantified with simple but high resolution modelling with the Bouguer-Lambert-Beer's law.

25 Using an extra-terrestrial solar spectrum of 0.05 nm resolution with a 0.01 nm increment (Egli, et al. 2013), together with ozone absorption coefficients for 223 K from Molecular Spectroscopy Lab, Institute of Environmental Physics (IUP), University of Bremen (Serdyuchenko, et al., 2011) interpolated from 0.02 nm to 0.01 nm resolution, and AOD following the Ångström law with the parameters $\alpha=1.3$ and $\beta=AOD_{1000nm}=0.012$, direct solar irradiance spectra at the surface were calculated for different airmasses and total column ozone amounts. In the calculations a station pressure of 770 hPa was used

30 which is close to the average value at the IZO station during the evaluated Langley plot events. Effective ozone altitude was set to 25 km and 22 km for calculations corresponding to measurements at Izaña and Davos, respectively. These values were also used for the Langley calibrations at Izaña (Sect 2.2) and for the AOD determinations in Davos (Sect. 5). For the relative optical airmass for ozone absorption the algorithm/formula by Komhyr et al. (1989) was used. Rayleigh optical depth, δ_R,

was calculated according to Bodhaine et al. (1999) and the relative optical airmass for Rayleigh scattering was calculated according to Kasten and Young (1989). The aerosol relative optical airmass, m_a, was estimated by an algorithm for water vapour airmass, m_w (Gueymard, 1995). The vertical distribution of the aerosol particles are generally not known but also in other AOD calculations the aerosol airmass have been approximated by m_w, e.g. for the GAW PFR network (McArthur et
5   al., 2003; Wehrli, 2008). Finally, the calculated irradiance spectra were convolved with the measured spectral response functions of UVPFR #1001.

Results of Langley plots of the simulated UVPFR direct irradiances were then compared to the extra-terrestrial irradiances calculated by convolving the extra-terrestrial spectrum with the UVPFR spectral response functions. The FWHM effect is mainly dependent on ozone amount and airmass range. For average conditions during the Langley calibrations at the IZO
10   station the V_0 correction factors were estimated to c_{FWHM}=[1.012 1.003 1.001 1.000] for the UVPFR channels from the shortest to the longest wavelength. These values are smaller but in line with corrections calculated for 2 nm FWHM using a more comprehensive model (Slusser et al., 2000). Accordingly, Langley extrapolation corrections found for the Brewer spectrophotometer (Gröbner and Kerr, 2001) are smaller than for the UVPFR at corresponding wavelengths, mainly due to the smaller FWHM (0.5–0.6 nm) of the Brewer.

15   Not only the derived V_0s are affected by the FWHM effect due to the rapidly changing ozone absorption with wavelength. Even if the correct V_0s are used, the calculated UVB AOD will still be incorrect if not a further correction is applied. With increasing airmass there is an increase in effective central wavelength for the sunphotometer channels as mentioned above. This results in an apparent decrease in ozone optical depth with increasing airmass. This effect was quantified by calculating the ozone optical depth from the modelled UVPFR direct irradiance signals using the Rayleigh and aerosol optical depth
20   values at their fixed effective central wavelengths. The effect varies slightly with station altitude/pressure. In Fig. 2, results are shown for an approximate pressure level in Davos (p= 840 hPa). The changes in effective ozone optical depth are strongest for the shortest wavelengths. The effect is negligible at the 332 nm wavelength.

The apparent change in ozone optical depth is not a perfect linear function with airmass. With little loss in accuracy, the ozone optical depth correction is still estimated as a linear function of m_o with the lines passing through the origin. The error
25   in the derived AOD using this simplification is according to the calculations performed here ≤0.001 units of AOD at the shortest wavelength and high total ozone amount, and considerably smaller at the other wavelengths and/or lower *TCO*. The resulting ozone optical depth correction factor for 350 DU total column ozone, $\Delta\delta_{o,350DU}$, is given in Table 2. The apparent decrease in ozone optical depth gets stronger with increasing total column ozone. The ozone optical depth change for 350 DU is taken as reference. Then the ratio of the ozone optical depth change at other ozone amounts at a specific m_o is very
30   similar for all wavelengths and can be approximated by a quadratic polynomial as

$$f_{o,DU} = \Delta\delta_{o,DU}/\Delta\delta_{o,350DU} = 6.1443 \cdot 10^{-6} \cdot TCO^2 + 0.8518 \cdot 10^{-3} \cdot TCO - 0.0513 \qquad (4)$$

where *TCO* is the total column ozone amount expressed in Dobson units. In this case, the coefficients in Eq. (4) are derived for a pressure of 840 hPa, corresponding to normal conditions in Davos. The resulting difference in $f_{o,DU}$ is negligible both for conditions at Izaña (about 770 hPa) and at sea level with differences in calculated AOD being less than 0.0005.

The Langley plot and AOD modelling was also made for a case with zero total column ozone. This showed that the FWHM

5 effects accounted for above practically entirely are caused by the rapidly increasing ozone absorption with decreasing wavelength.

All in all, at an airmass of 2 and total column ozone amount of 350 DU the effect of the FWHM corrections on derived AOD at 305 nm is about +0.015, while it is only about +0.004 at 311 nm. Both these values are much lower than the total uncertainty in the UV AOD (see Sect. 4 below) but since the errors due to the finite FWHM are systematic the relatively

10 small corrections are still performed (GUM, 2008).

3 Calculation of AOD from UVPFR measurements

A more detailed form of the Bouguer-Lambert-Beer law in equation 1, valid at a (monochromatic) UVPFR wavelength λ, is

$$\ln(V_\lambda) = \ln(R^2 V_{0,\lambda}) - m_R \delta_{R,\lambda} - m_o \delta_{o,\lambda} - m_a \delta_{a,\lambda} - m_n \delta_{n,\lambda} - m_s \delta_{s,\lambda} \tag{5}$$

Solving for aerosol optical depth, $\delta_{a,\lambda}$, and neglecting the assumed very small optical depths due to absorption in NO_2 ($\delta_{n,\lambda}$) and SO_2 ($\delta_{s,\lambda}$) while including the FWHM corrections described above, leads to

$$AOD_\lambda = \delta_{a,\lambda} = \ln\left(\frac{C_{FWHM,\lambda} V_{0,\lambda}}{R^2 V_\lambda}\right)\Big/ m_a - \frac{m_R}{m_a}\frac{p}{p_0}\delta_{R,\lambda} - \frac{m_o}{m_a}\left(\delta_{o,\lambda} + f_{o,DU}\Delta\delta_{o,\lambda,350DU}m_o\right) \tag{6}$$

from the measurement of one of the spectral UVPFR output signals V_λ. The $V_{0,\lambda}$ is the calibration constant at the same wavelength derived from the Langley plot calibrations as described above. Air pressure, *p*, is also measured at the station and p_0= 1013.25 hPa is the standard pressure at sea-level.

The ozone optical depth, $\delta_{o,\lambda}$, is calculated from ozone absorption coefficients, $k_{o,\lambda}$, and *TCO* amount. The ozone absorption

25 coefficients are based on ozone cross section data determined by Bass and Paur (1985) which are also used for the operational ozone determinations by Brewer spectrophotometers. The effective ozone temperature and altitude are also approximated in the same way as for the operational ozone amount determinations, i.e. by the constant values -45 °C and 22 km, respectively. Values on $k_{o,\lambda}$ for the UVPFR #1001 are given in Table 2.

Indeed, using other datasets on ozone cross sections would result in different AOD values, especially at the shortest

30 wavelengths. The effect of different cross sections is not further investigated here. In any case the same cross sections should be used for both *TCO* and AOD determinations.

The ozone amounts taken from a collocated Brewer are calculated with more recent Rayleigh scattering coefficients instead of the standard ones used in the operational Brewer program. As an example, for Brewer #163 in Davos the corrected *TCO* values are 2.7 DU lower than the operational ones.

The other parameters on the right-hand side of Eq. (6) are calculated mainly from position and time and the applied airmass formulas were given in Sect. 2.3 above. As above, Rayleigh optical depth, $\delta_{R,\lambda}$, is calculated with the Bodhaine et al. (1999) algorithm. (In this case, the *p/p₀* factor is already included in the resulting $\delta_{R,\lambda}$.) Potential absorption in NO_2 and SO_2 is not included in Eq. (5). The actual amounts of these gases over the measurement site(s) are not known but are assumed to be negligibly small. The potential error of this simplification is quantified in the next section.

AOD values calculated by Eq. (6) are only valid for times when there are no clouds in front of the sun. The cloud screening applied in this study is based on the method by Alexandrov et al. (2004) with modifications to fit the UVPFR measurements.

4 AOD uncertainty

A simplified uncertainty analysis has been made for the AOD values retrieved from a UVPFR sunphotometer. The law of propagation of uncertainties for independent variables states that for the combined standard uncertainty of the measurand estimate *y*, $u_c(y)$,

$$u_c{}^2(y) = \sum_{i=1}^{N} \left(\frac{\partial f}{\partial x_i}\right)^2 u^2(x_i) \tag{7}$$

where $u(x_i)$ is the standard uncertainty of each input variable x_i (GUM 2008). For the $AOD_\lambda = \delta_{a,\lambda}$ calculated according to equation 5 this translates to

$$u_c(\delta_{a,\lambda}) = \left\{ \left[\frac{1}{m_a}\frac{u(V_{0,\lambda})}{V_{0,\lambda}}\right]^2 + \left[\frac{1}{m_a}\frac{u(R^2)}{R^2}\right]^2 + \left[\frac{1}{m_a}\frac{u(V_\lambda)}{V_\lambda}\right]^2 + \left[\frac{1}{m_a}\frac{u(V_{CS,\lambda})}{V_{CS,\lambda}}\right]^2 + \left[\frac{m_R}{m_a}u(\delta_{R,\lambda})\right]^2 + \left[\frac{m_o}{m_a}u(\delta_{o,\lambda})\right]^2 + \left[\frac{m_N}{m_a}u(\delta_{N,\lambda})\right]^2 + \right.$$

$$\left. + \left[\frac{m_S}{m_a}u(\delta_{S,\lambda})\right]^2 + \left[\delta_{a,\lambda}\frac{u(m_a)}{m_a}\right]^2 + \left[\delta_{R,\lambda}\frac{u(m_R)}{m_a}\right]^2 + \left[\delta_{o,\lambda}\frac{u(m_o)}{m_a}\right]^2 \right\}^{1/2}$$

$$\tag{8}$$

For simplicity, the contribution due to correlated variables has been omitted. Similar AOD uncertainty expressions can be found in the literature (e.g. Russel et al., 1993; Carlund et al., 2003;). A slightly different approach was taken by Mitchell and Forgan (2003) where they investigated uncertainty in total optical depth from different sunphotometers measuring at similar wavelengths. When using Eq. (8), uncertainty of c_{FWHM} is included in the $u(V_{0,\lambda})$ uncertainty and uncertainty contributions from $f_{o,DU}$ and $\Delta\delta_{o,\lambda,350DU}$ are included in the $u(\delta_{o,\lambda})$ term. To get the expanded uncertainty, *U*, the combined standard uncertainty ($u_c(\delta_{o,\lambda})$) is multiplied by a coverage factor, *k*. In this case *k*=2 is chosen to get an approximate level of confidence of 95 %. So

$$U_{95} = k \cdot u_c(\delta_{a,\lambda}) = 2 \cdot u_c(\delta_{a,\lambda}) \tag{9}$$

for a number of effective degrees of freedom of $u_c(\delta_{a,\lambda})$ of significant size (>50), which is here the case.

4.1 Uncertainty of ozone optical depth

At the shortest UVPFR wavelengths the most dominant source of uncertainty in AOD determinations originates from the uncertainty in ozone optical depth. In the $u(\delta_{o,\lambda})$, contributions from ozone cross section related uncertainty, uncertainty in total column ozone amount and effective ozone temperature are taken into account. Bass and Paur only report 1% noise during their measurements (Bass and Paur, 1985). Gorshelev et al. (2014) estimate that the total uncertainty in the Bass and Paur cross sections exceeds 2 %. Serdyuchenko et al. (2011) state that a 3 % accuracy has been achieved for their (IUP Bremen) ozone cross sections and Gorshelev et al. (2014) state 2-3 % total uncertainty for the wavelength region under consideration here. Recently, Weber, et al. (2016) reviewed the uncertainty of ozone cross datasets and found a 2.1 % overall uncertainty of the Bass and Paur cross sections in the Huggins band up to about 330 nm. From this, $u(\delta_{o,\lambda,XS})$=2.1 % (1σ, normal distribution) is here assumed for all UVPFR wavelengths. For the ozone amount 1 % (1σ, normal distribution) is taken as the standard uncertainty $u(\delta_{o,\lambda,DU})$. The estimated uncertainty in effective ozone temperature, $u(\delta_{o,\lambda,T})$, is a function of latitude and month. At low latitudes the day-to-day variation in effective ozone temperature is low. From 30° latitude and below, the uncertainty in effective ozone temperature is estimated to 5°C (95 % confidence level, normal distribution). At high latitudes the uncertainty is up to 10°C most of the year, with slightly lower values in June-August. For latitudes between 30°-80° the uncertainty changes from the lower to the higher values. The total standard uncertainty connected ozone optical depth is calculated as

$$u(\delta_{o,\lambda}) = \left(u(\delta_{o,\lambda,XS})^2 + u(\delta_{o,\lambda,DU})^2 + u(\delta_{o,\lambda,T})^2 \right)^{1/2} \tag{10}$$

The uncertainty in the relatively small contributions from the FWHM correction of the ozone optical depth ($u(f_{o,DU})$ and $u(\Delta\delta_{o,\lambda,350DU})$) are considered to be covered in the total uncertainty based on the other ozone uncertainty terms.

4.2 Uncertainty of calibration

In the V_0 uncertainty, one contribution comes from the spread in the Langley plot results. The 27 Langley plot cases available from 2015 are not many enough to really determine the actual distribution of the V_0s. Not even with the additional 12 cases from 2016, for the two wavelengths with nearly no change in sensitivity over more than a year, it is possible to determine the actual distribution. From the derived histograms either a normal or a triangular distribution is plausible. As a matter of precaution, a triangular distribution is assumed for the V_0s. It is hoped that this will also cover the uncertainty of

the calibration method that may have been introduced by e.g. the subjective Langley event selection by the analyst. Values close to the maximum and minimum of the individual Langley plot V_0s are taken as limits, resulting in an estimated standard uncertainty due to spread in the Langley plot V_0s of $u(V_{0,\lambda,L})$=[2.2 1.3 1.7 1.1]/$\sqrt{6}$ %. (Terms within brackets are here and in the following listed from the shortest to the longest UVPFR wavelength).

5   Contributing to the V_0 related uncertainty, there is also uncertainty added due to a possible ozone change during the Langley plot periods not accounted for. In this respect, the systematic effect of a 0.5 DU change during each Langley plot event, made over an air mass range of 1.5, was estimated using the results in Fig. 1. This corresponds approximately to a 0.25 % mean error in the extra-terrestrial constant of the Brewer triad instruments, which is considered as a maximum value based on RBCC-E results (WMO/GAW, 2015). The values [0.7 0.3 0.1 0.05]/1.5 % were taken as semi ranges of rectangular

10 distributions for the UVPFR wavelengths, resulting in standard uncertainties of $u(V_{0,\lambda,o})$=[0.47 0.20 0.07 0.03]/$\sqrt{3}$ %.

Also uncertainties in the c_{FWHM} factors have been accounted for. The values $u(V_{0,\lambda,FWHM})$=[0.0040 0.0015 0.0005 0.0002]/$\sqrt{3}$ were estimated in this case.

Any additional uncertainty in V_0 due to a possible systematic effect in m_R has not been taken into account. Also, the effect of unknown vertical aerosol distribution on the derived Langley V_0 was tested by assuming m_a=m_R, instead of the used

15 algorithm for m_a. The result was only a negligible influence on the V_0s. As mentioned above, in the calculations of m_o for Langley plots at IZO, effective ozone altitude of 25 km was used. For ozone determination by Dobson spectrophotometers, an ozone layer altitude of about 23 km is recommended for the latitude of the IZO station (WMO/GAW, 2009). Assuming a systematically over- or underestimation of ozone altitude of 2 km resulted in the standard uncertainty of $u(V_{0,\lambda,o3alt})$=[0.6 0.3 0.1 0.02]/$\sqrt{3}$ %.

20 As mentioned above, there is a large uncertainty in ozone optical depth at wavelengths with high ozone absorption. While this adds some uncertainty to V_0s of the refined Langley plot method, fortunately, the additional uncertainty in V_0 from the Langley method of Eq. (3) is negligible. Ozone optical depth is only used for the air mass weighting in this case.

Finally, a drift term of $u(V_{0,drift})$=1 % per year (95 % confidence level, normal distribution) has been accounted for in the total V_0 uncertainties. In the end, $u(V_{0,\lambda})$ is calculated as

25 $$u(V_{0,\lambda}) = \left(u(V_{0,\lambda,L})^2 + u(V_{0,\lambda,o})^2 + u(V_{0,\lambda,FWHM})^2 + u(V_{0,\lambda,o3alt})^2 + u(V_{0,\lambda,drift})^2 \right)^{1/2} \qquad (11)$$

4.3 Uncertainty of Rayleigh optical depth

The standard uncertainty of the Rayleigh optical depth, $u(\delta_{R,\lambda})$, was derived from a 1 hPa pressure uncertainty (1σ) and difference between $\delta_{R,\lambda}$ (Bodhaine et al., 1999) and the extreme values calculated for other model atmospheres by Tomasi et al. (2005, Table 5). These latter differences were taken as limits of a 95 % confidence interval of a normal distribution.

4.4 Uncertainty of measured signal including circumsolar contribution

Uncertainty in voltage readings, $u(V_\lambda)$, is calculated according to the specification of the CR10X logger for the temperature range -25°C to 50°C. The uncertainty due to additional circumsolar radiation seen within the field of view of the UVPFR, $u(V_{CS,\lambda})$, is based on the results found by Russel et al. (2004) and interpolated and extrapolated to UVPFR field of view and

5   wavelengths. These results are further increased by a factor of 1.25 to fit circumsolar radiation levels modelled with the SMARTS2 model (Gueymard, 1995). These results are directly expressed as an AOD uncertainty due to circumsolar radiation in the FOV, $u(\delta_{a,\lambda,CS})$, and it depends on wavelength, Ångström's wavelength exponent α and AOD amount. Therefore, the fourth term on the right hand side of Eq. (8) is replaced by $u(\delta_{a,\lambda,CS})$.

This way of estimating the additional diffuse light entering the instrument does not result in a bias of calibration through

10   Langley plots, since it is not dependent on air mass. This is probably not the case in reality. As suggested by Arola and Koskela (2004) diffuse light could introduce a significant negative bias in Langley plot results at UVB wavelengths under high AOD conditions. The average UVB AOD during the Langley calibrations of the UVPFR at Izaña was only about 0.05. At the same time, the average of Ångström's wavelength exponent calculated from AOD in the 368-862 nm range was about 1.5 during the Langley plot events, which indicates that the aerosol forward scattering was not particularly high. In addition,

15   the maximum air mass during Langley plots never exceeded 3. It is therefore assumed that the diffuse light influence was very small on the UVPFR calibrations. Hence, this source of uncertainty was not specifically taken into account in the already conservative V_0 uncertainty estimation above.

4.5 Uncertainty due to neglected gaseous absorption

Absorption in NO_2 peaks around 400 nm but there is also some absorption at the UVPFR wavelengths, especially at the

20   longest one. The amount of NO_2 in the atmosphere over the measuring site is unknown. In many model reference atmospheres, the total column NO_2 is about 0.2 DU (=$2\cdot10^{-4}$ atm cm) (Gueymard 1995), corresponding to $5.37\cdot10^{15}$ molecules cm^{-2}. If this is taken as standard uncertainty of NO_2 amount, the approximate 95 % confidence level NO_2 amount becomes more than $10\cdot10^{15}$ molecules cm^{-2}. From OMI overpass data on total column NO_2 (http://www.temis.nl/airpollution/no2col/overpass_no2.html), it is concluded that at both Izaña and Davos the total column

25   NO_2 should be less than $10\cdot10^{15}$ molecules cm^{-2} more than 95 % of the time. The NO_2 amount in the AERONET monthly climatology, based on the SCHIAMACHY dataset set (http://aeronet.gsfc.nasa.gov/version2_table.pdf and references therein), is also about 0.2 DU in Davos for the measurement periods analysed in this work. Hence, to calculate the standard uncertainty in NO_2 optical depth, $u(\delta_{N,\lambda})$, the NO_2 absorption coefficients at the UVPFR wavelengths where taken from the SMARTS2 model and multiplied by 0.2 DU NO_2. The assumption is that uncertainty in both NO_2 amount and absorption

30   coefficients is covered by this estimate.

For the calculation of the standard uncertainty due to neglecting absorption in SO_2, cross sections for SO_2 (valid at 195 K) determined by Vandaele et al. (1994) were used. (This data set is available at the IUP University of Bremen website

http://www.iup.uni-bremen.de/gruppen/molspec/databases/dlrdatabase/sulfur/index.html.) Brewer spectrophotometers are also capable of measuring columnar SO_2 amounts. However, due to the relatively high noise levels of 1-2 DU for these measurements, they can not be used to accurately determine the normal low background SO_2 levels. Increased SO_2 levels due to e.g. volcanic eruptions are however detectable (e.g. Zerefos et al. 2016). During the UVPFR measurements at Izaña

5 and in Davos, the co-located Brewers indeed measured average SO_2 values close to zero (or even slightly negative) with standard deviation <1 DU. It is therefore estimated that for the uncertainty analysis it is sufficient to use a SO_2 value of 0.25 DU (1σ, normal distribution) when calculating the standard uncertainty $u(\delta_{S,\lambda})$.

Not taking NO_2 and SO_2 absorption and circumsolar radiation into account introduces biases in the derived AOD_λ values. However, these biases are of different sign and therefore cancel out each other to some extent. In this example the sum of

10 $u(\delta_{N,\lambda})$ and $u(\delta_{S,\lambda})$ equals [0.0030 0.0024 0.0017 0.0019], while the $u(\delta_{a,\lambda,CS})$=[0.0034 0.0033 0.0031 0.0029] at the nominal UVPFR wavelengths [305 311 317 332] nm. Still, in the calculation of the combined standard uncertainty these uncertainty sources are all added.

4.6 Uncertainty in solar position and air mass terms

Based on comparison between R^2 calculated in solar position algorithms by Michalsky (1988) and Reda and Andreas (2003,

15 revised 2008) the uncertainty in sun-earth distance correction factor was estimated to $u(R^2)$=0.0003.

The actual vertical distribution of gases and aerosol particles in the atmosphere is not known. This introduces uncertainties in the relative optical air masses used for AOD calculation. As necessary input to the airmass algorithms the true or apparent solar zenith angle is given which is also calculated with a small uncertainty. For the UVPFR analysis the solar position algorithm by Reda and Andreas (2003, revised 2008) is used. According to the authors this algorithm is accurate within

20 0.0003° over eight millennia in time. This should be valid for the true solar zenith angle since the actual refraction is not known in every case. The Reda and Andreas algorithm was compared to the solar position calculations operational at PMOD/WRC for the evaluation of standard PFR measurements which utilise the solar position calculation algorithm by Montenbruck and Pfleger (1994) with refraction correction by Meeus (1991). These algorithms were always found to agree within 0.01° for tests over a number of days during different years and at different locations and altitudes. Since the UVPFR

25 AOD determinations are limited to solar zenith angles <75°, when the differences in refraction for different atmospheric temperatures is small, the uncertainty in solar zenith angle input to air mass calculations is estimated to 0.01° (95 % confidence level, rectangular distribution).

The air mass term thought to be the least uncertain is the air mass for Rayleigh scattering, m_R. According to Kasten and Young (1989) their relative optical air mass formula deviates <0.07 % from more rigorous calculations at m_R <7. Twice this

30 value is taken as a 95 % confidence limit for a rectangular distribution. For the total standard uncertainty $u(m_R)$ the contributions due to uncertainty in SZA and due to algorithm uncertainty are simply added like

$$u(m_R) = 0.0014 m_R/\sqrt{3} + \left(m_R(SZA_a + 0.01°) - m_R(SZA_a)\right)/\sqrt{3} \qquad (12)$$

where SZA_a is the apparent solar zenith angle. The uncertainty in relative optical airmass for ozone is calculated by assuming that the effective ozone altitude differs ≤4 km from the used value 22 km in 95 % of the cases. So,

$$5 \quad u(m_o) = \big(m_o(18\,km) - m_o(22\,km)\big)/2 \qquad (13)$$

A 4 km uncertainty (2σ, normal distribution) in the effective ozone altitude is thought to be a conservative estimate for the two sites where the UVPFR has been operating, therefore an extra contribution from a small error in true solar azimuth angle input to the ozone airmass calculation is omitted.

In this study the vertical aerosol particle distribution is assumed to be more concentrated near the ground than the vertical distribution of the molecules of the air, leading to $m_a > m_R$. This is probably a good assumption in many situations without volcanic aerosols in the stratosphere. Nevertheless, there will be uncertainty in m_a due to the unknown vertical aerosol distribution. It is estimated that the difference between m_a and m_R can be taken as a 95 % confidence limit of a rectangular distribution of the uncertainty of m_a due to unknown vertical distribution of the aerosol. Like for $u(m_R)$ also a contribution from SZA_a uncertainty is added leading to

$$u(m_a) = (m_a - m_R)/\sqrt{3} + \big(m_a(SZA_a + 0.01°) - m_a(SZA_a)\big)/\sqrt{3} \qquad (14)$$

20 **4.7 Total UVPFR AOD uncertainty**

In Fig. 3 the estimated expanded uncertainty (U_{95}) and the individual uncertainty components, the terms on the right hand side of Eq. 8, are shown for an example case over the airmass range 1–3.8. Calculations are made for measurements near sea level and a total column ozone amount of 350 DU. The AOD values used at the four wavelengths are given in the graphs which corresponds to the parameters α=1.3 and β=AOD$_{1000nm}$=0.040 in the Ångström power law. The resulting UV AOD values are about twice as high as the mean AOD values during the measurements in Davos presented below. Both the expanded uncertainties as well as the individual uncertainty values are given for an approximate level of confidence of 95 % in the figure.

Clearly, the dominant part of the AOD uncertainty is caused by the uncertainty in the ozone optical depth at the three shortest wavelengths. As the absorption by ozone decreases with wavelength the size of the $u(\delta_{o,\lambda})$ uncertainty also strongly decreases. For the longest wavelength the major contribution at low airmasses comes from the calibration uncertainty in this analysis. This is also the source of uncertainty with the strongest airmass dependence due to the $1/m_a$ reduction factor.

Major contributions to these uncertainties come from (unknown) systematic effects. Therefore, the uncertainty of average AOD values based on a high number of measurements does not decrease as much as with the factor $1/\sqrt{N}$.

It is believed that the most dominant uncertainties have been included in the current analysis. However, in addition to neglecting the effect of correlated variables, there are still some uncertainty sources which have not been taken into account

5   when calculating the total uncertainties. For example, no information on potential non-linearity in the voltage output from the UVPFR has been found. This source of uncertainty is assumed to be small and has therefore been neglected. The pointing accuracy is monitored with the UVPFR. Normally, the pointing error is ≤0.2°. Any uncertainty caused by 0.2° pointing error has not been taken into account. Probably more importantly, no uncertainty contributions from potential errors in the used spectral response functions have been taken into account.

10   For the two shortest wavelengths the estimated AOD uncertainties are very high, which of course is not very encouraging. At the same time, the estimated 2σ uncertainty at 305 nm is still only about half of estimates by Kazadzis, et al. (2005) who estimated 1σ uncertainty at UVB wavelengths to 0.07. It is therefore considered useful to continue working on AOD even at 305-306 nm to learn more on AOD retrievals in the UVB. Probably, better input information/data will be available in the future which will reduce the AOD uncertainty. If algorithms and coefficients in the AOD calculations are standardized in a

15   network of stations, which will be the case within e.g. EUBREWNET (http://rbcce.aemet.es/eubrewnet), the precision of derived AOD values will still be high for well-maintained measurements.

5. UV AOD observations in Davos

After the calibration at Izaña in summer 2015 the UVPFR has been operated about two months during autumn 2015 and spring 2016, respectively, at PMOD/WRC in Davos. These measurements were analysed to show an example of AOD

20   determination with the UVPFR. The calibration results from 2015 have been used for the whole period in Davos.

As a first result cloud screened 1-minute AOD values from UVPFR #1001 during the day 12 October 2015 in Davos are shown in Fig. 4. AOD from PFR-N24, one of the standard PFR triad instruments (wavelengths 368, 412, 500 and 862 nm), are also shown in the graph. This day the turbidity in Davos was very low, which rather frequently occurs at high altitude stations. Under these conditions the effect of the FWHM corrections of the UVPFR data becomes extra important. From the

25   near infrared to the UVB range AOD increases with decreasing wavelength, according to the results in Fig. 4. Without the FWHM corrections this would not have been the case in the UV. AOD at 305 nm would the whole day have been lower than at 332 nm and often even lower than at 368 nm. AOD at 311 nm would also have been lower than at 318 nm the whole day. Based on these results for low turbidity conditions it is assumed that AOD from the UVPFR really do become more realistic when the proposed FWHM corrections are applied.

30   Daily means of cloud screened 1-minute AOD values at the 305 nm and 332 nm wavelengths are shown to the left in Fig. 5. The averages of the daily mean AODs at all the UVPFR wavelengths, as well as from the PFR-N24, are shown to the right. Clearly, very low values of AOD are often experienced over Davos, even at UVB wavelengths. Especially during autumn

2015 this was the case. In spring 2016, the turbidity conditions were more variable. The average AOD values for the whole period were measured lower than 0.1 at all four UVPFR wavelengths. During this period the average AOD values in the UVB are not very well estimated by extrapolating AOD values at the UVA-NIR wavelengths using the common Ångström relation, represented by the (red) full line in the right panel of Fig. 5. More specific extrapolated AOD at UV wavelengths is overestimated. Using a second order fit in the log-log space leads to much better results. As shown above, the uncertainties of the UV AOD values are however considerable and the AOD values measured by the UVPFR are not significantly different from any of the extrapolated values in this low turbidity case.

In the calibration section above (Sect. 2.2) the UVPFR sensitivity was shown to be satisfactorily stable over one year. As an additional stability and consistency check AOD from the UVPFR has been compared to AOD derived from a Brewer spectrophotometer. At PMOD/WRC the Brewer Mk III #163 is operated. This instrument provided the ozone values used in the AOD calculations based on spectral transmission data from the UVPFR in Davos.

Both Brewer #163 and the UVPFR #1001 participated in the 10th RBCC-E campaign 27 May – 4 June 2015 at the INTA (Instituto de Técnica Aerospacial) El Arenosillo station in southern Spain (37.10° N, 6.73° W, 41 m). In addition to the regular calibration of the ozone measurements during this RBCC-E campaign, Brewer #163 was also absolutely calibrated for AOD determinations versus the UVPFR #1001. Using this calibration, UV AOD has been determined from Brewer #163 during its measurements in Davos. Also a small temperature correction was applied to the Brewer direct irradiance readings as well as a polarization correction suggested by Cede et al. (2006).

The comparison of AOD from Brewer #163 and the UVPFR #1001 in Davos is shown in Fig. 6. Since the UVPFR has the highest sampling rate (1 measurement/minute) UVPFR AODs were first interpolated (linearly) to Brewer direct sun (DS) measurement times. These UVPFR AOD values at Brewer DS times were then further interpolated from the nearest surrounding UVPFR wavelength pair to the Brewer wavelengths using the Ångström relation.

Individual AOD differences (UVPFR-Brewer) for cloud screened and near simultaneous measurements are shown in Fig. 6. In the graphs, also the suggested WMO traceability limits for absolute AOD differences (that have been defined for AOD at wavelengths without gaseous absorption in the UVA-NIR wavelengths range) are shown. Obviously, the agreement is very good between the Brewer and the UVPFR for these measurements taken 4-11 months after the calibration. At four of the five Brewer wavelengths more than 95 % of the differences fall within the WMO limits. Only at the shortest wavelength, with 85.6 % of the differences within the limits, the traceability requirement of 95 % was not fulfilled. This indicates a small change in any of the instruments at the shortest wavelength(s). The root mean squared difference is still low at all wavelengths, amounting to [0.008, 0.006 0.006 0.005 0.005] for the 306-320 nm wavelengths.

6. Conclusions

This paper reports on the UVPFR sunphotometer, an instrument that can be used for aerosol optical depth measurements at four UV wavelengths. The standard PFRs were designed with emphasis on precision and stability, while also being robust

instruments. These goals have been reached by the PFRs (Wehrli 2000; Gröbner et al., 2015;). The UVPFR is of similar design and based on the results of this first study, including suggested corrections, the UVPFR appear to be a stable high quality radiometer for AOD determinations in the UV. According to Langley plot calibrations at a high altitude station the sensitivity of the UVPFR changed by ≤1.1 % over a 13-14 month period.

5   It was shown that due to the relative wide FWHM of the UVPFR the calibration constants (V_0) from Langley plot calibrations underestimate the true extra-terrestrial signals. Accordingly, correction factors were suggested. The effect of the finite FWHM is an apparent wavelength shift towards longer wavelengths as airmass increases, especially for the shorter UVPFR wavelength channels 305 nm and 311 nm. This also results in an apparent decrease in ozone optical depth with increasing airmass. An adjusted formula for the calculation of AOD with a correction term dependent on total column ozone

10   amount and ozone air mass (Eq. 6) was therefore developed.

Even with the suggested corrections applied, the expanded uncertainty of AOD derived from UVPFR measurements, as well as from other UVB instruments, remains relatively high at the shortest wavelengths. The major source of uncertainty is the ozone optical depth uncertainty, resulting from ozone cross section uncertainty and ozone temperature and total column amount uncertainties. The next largest source of uncertainty at the three shortest wavelengths, and the largest source of

15   uncertainty at 332 nm, is the calibration uncertainty, especially at high sun/low airmass conditions.

Despite the relatively high AOD uncertainties at the short wavelengths, it is still considered worthwhile to continue working with the AOD at e.g. 305-306 nm to learn more on AOD retrievals in the UVB. Most probably, better input information connected to ozone will be available in the future which will reduce the AOD uncertainty. Also, if the same ozone cross section data and effective ozone temperature data are used by different instruments/groups/sites, as will be the case within

20   EUBREWNET for example, the AOD results will be consistent and much more comparable.

An example of very good agreement of UV AOD retrievals was shown by a comparison between the UVPFR #1001 and Brewer #163 for several months of measurements in Davos. Since Brewer #163 and UVPFR #1001calibrations were partly linked at an earlier date, the comparison was not performed by fully independent instruments and therefore we should expect a relatively good agreement. The comparison indeed confirms good agreement and for the measurements taken 4-11 months

25   after the Brewer calibration. The root mean squared AOD differences were <0.01 at all the 306-320 nm Brewer wavelengths. This can be considered a very good result for an AOD comparison at UVB wavelengths. An additional very likely reason for the good agreement is the fact that both instrument types measure at close wavelengths in the UVB. In earlier studies in which AOD was determined from Brewer direct sun measurements the validation has so far only been done against measurements at UVA or even visible wavelengths (Marenco et al., 2002; Cheymol and De Backer, 2003; Cheymol et al.,

30   2006; Gröbner and Meleti, 2004; Kazadzis et al. 2005; Kazadzis et al. 2007; De Bock et al., 2010; Kumharn et al., 2012;). Also earlier comparisons of AOD from Brewers of different type have shown larger differences than between the UVPFR and the MkIII Brewer in this study (Kazadzis et al. 2005; Kumharn et al., 2012;).

In addition to a low turbidity case showing AOD values from the UVPFR consistent with a standard PFR, average UV AOD values of the UVPFR during the measurements in Davos were compared with highly accurate AOD values, 2σ uncertainties

estimated to <0.01, at UVA-NIR wavelengths from a standard PFR. Extrapolated AODs at UVPFR wavelengths using a second order polynomial fit of log(AOD) versus log(λ) were closer to the mean values measured by the UVPFR than when a first order fit, i.e. the common Ångström relation, was used for extrapolation. However, in both cases the difference between the extrapolated and the measured values were smaller than the estimated UVPFR AOD uncertainties for the low AOD conditions experienced during the measurements in Davos.

Despite the fact that the total uncertainty of AOD in the UVB is relatively high, based on the comparison between the UVPFR and a Brewer it is estimated that calibrated and well maintained UVPFR sunphotometers and Brewer spectrophotometers can measure AOD at a precision of 0.01 (1σ) at their direct sun measurement wavelengths.

Data availability

The total column ozone data used in this study can be downloaded from the EUBREWNET website: http://rbcce.aemet.es/eubrewnet.

Acknowledgements

T. Carlund was supported through Grant Nr. C14.0025 from the Swiss Staatssektretariat für Bildung, Forschung und Innovation (SBFI) within COST ES1207. Part of the work was supported by a STSM Grant from COST Action ES1207 (EUBREWNET – A European Brewer Network). The slit function measurements were done on the tuneable laser facility ATLAS, funded through contract number IDEAS+/SER/SUB/11. The total column ozone values from the Brewer triad at the Izaña observatory were kindly provided by Alberto Redondas at IARC/AEMET.

References

Alexandrov, M. D., Marshak, A., Cairns, B., Lacis, A. A., and Carlson, B. E. : Automated cloud screening algorithm for MFRSR data, Geophys. Res. Lett., 31, L04118, doi:10.1029/2003GL019105, 2004.

Arola, A. and Koskela, T.: On the sources of bias in aerosol optical depth retrieval in the UV range, J. Geophys. Res., 109, D08209, doi:10.1029/2003JD004375, 2004.

Bass, A. M. and Paur, R. J.: The ultraviolet cross-sections of ozone. I. The measurements, II. Results and temperature dependence, in: Atmospheric ozone; Proceedings of the Quadrennial ozone symposium, 1, 606–616, 1985.

Bodhaine, B. A., Wood, N. B., Dutton, E. G., and Slusser, J. R.: On Rayleigh optical depth calculations, J. Atmos. Ocean. Tech., 16(11), Part 2, pp 1854–1861, 1999.

Carlund, T., Landelius, T., and Josefsson, W.: Comparison and uncertainty of aerosol optical depth estimates derived from spectral and broadband measurements. J. Appl. Meteorol., 42(11), 1598–1610, 2003.

Cede, A., Labow, G., Kowalewski, M., and Herman, J.: The effect of polarization sensitivity of Brewer spectrometers on direct Sun measurements, in: Ultraviolet Ground- and Space-Based Measurements, Models, and Effects IV, Proc. SPIE Int. Soc. Opt. Eng., 5545, 131–137, 2004.

Cede, A., Kazadzis, S., Kowalewski, M., Bais, A., Kouremeti, N., Blumthaler, M., and Herman, J.: Correction of direct irradiance measurements of Brewer spectrophotometers due to the effect of internal polarization, Geophys. Res. Lett., 33, L02806, doi:10.1029/2005GL024860, 2006.

Cheymol, A. and De Backer, H.: Retrieval of the aerosol optical depth in the UV-B at Uccle from Brewer ozone measurements over a long time period 1984-2002. J. Geophys. Res., 108, 4800, doi:10.1029/2003JD003758, 2003.

Cheymol, A., De Backer, H., Josefsson, W., and Stübi, R.: Comparison and validation of the aerosol optical depth obtained with the Langley plot method in the UV-B from Brewer Ozone Spectrophotometer measurements. J. Geophys. Res., 111, D16202, doi:10.1029/2006JD007131, 2006.

Cordero, R. R., Seckmeyer, G., Pissulla, D., and Labbe, F.: Exploitation of spectral direct UV irradiance measurements, Metrologia, 46, 19–25, doi:10.1088/0026-1394/46/1/003, 2009.

Corr, C. A., Krotkov, N., Madronich, S., Slusser, J. R., Holben, B., Gao, W., Flynn, J., Lefer, B., and Kreidenweis, S. M.: Retrieval of aerosol single scattering albedo at ultraviolet wavelengths at the T1 site during MILAGRO, Atmos. Chem. Phys., 9, 5813–5827, doi:10.5194/acp-9-5813-2009, 2009.

De Bock, V., De Backer, H., Mangold, A., and Delcloo, A.: Aerosol optical depth measurements at 340 nm with a Brewer spectrophotometer and comparison with Cimel sunphotometer observations at Uccle, Belgium. Atmos. Meas. Tech., 3, 1577–1588, doi: 10.5194/amt-3-1577-2010, 2010.

De Bock, V., De Backer, H., Van Malderen, R., Mangold, A., and Delcloo, A.: Relations between erythemal UV dose, global solar radiation, total ozone column and aerosol optical depth at Uccle, Belgium. Atmos. Chem. Phys., 14, 12251–12270. doi:10.5194/acp-14-12251-2014, 2014.

Diémoz, H., Eleftheratos, K., Kazadzis, S., Amiridis, V., and Zerefos, C. S.: Retrieval of aerosol optical depth in the visible range with a Brewer spectrophotometer in Athens, Atmos. Meas. Tech., 9, 1871–1888, doi:10.5194/amt-9-1871-2016, 2016.

Diffey, B. L.: Solar ultraviolet radiation effects on biological systems, Phys. Med. Biol., 36(3), 299–328, doi:10.1088/0031-9155/36/3/001, 1991.

Eck, T. F., Holben, B. N., Reid, J. S., Dubovik, O., Smirnov, A., O'Neill, N. T., Slutsker, I., and Kinne, S.: Wavelength dependence of the optical depth of biomass burning, urban and desert dust aerosols, J. Geophys. Res., 104, D24, 31333–31349, 1999.

Egli, L., Gröbner, J., and Shapiro, A.: Development of a new high resolution extraterrestrial solar spectrum. PMOD/WRC Annual report 2012, available at: http://www.pmodwrc.ch/annual_report/2012_PMODWRC_Annual_Report.pdf, last access: 20 October 2016, 2013.

Fioletov, V. E., Kerr, J. B., McElroy, C. T., Wardle, D. I., Savastiouk, V., and Grajnar, T. S.: The Brewer reference triad, Geophys. Res. Lett., 32, L20805, doi:10.1029/2005GL024244, 2005.

Forgan, B. W.: Bias in a solar constant determination by the Langley method due to structured atmospheric aerosol: comment, Appl. Optics, 27(12), 2546–2548, 1988.

Gerasopoulos, E., Kazadzis, S., Vrekoussis, M., Kouvarakis, G., Liakakou, E., Kouremeti, N., Giannadaki, D., Kanakidou, M., Bohn, B., and Mihalopoulos, N.: Factors affecting O3 and NO2 photolysis frequencies measured in the eastern Mediterranean during the five year period 2002–2006, J. Geophys. Res., 117, D22305, doi:10.1029/2012JD017622, 2012.

Gorshelev, V., Serdyuchenko, A., Weber, M., Chehade, W., and Burrows, J. P.: High spectral resolution ozone absorption cross sections – Part 1: Measurements, data analysis and comparison with previous measurements around 293 K, Atmos. Meas. Tech., 7, 609–624, doi:10.5194/amt-7-609-2014, 2014.

Gröbner, J. and Kerr, J.B.: Ground-based determination of the spectral ultraviolet extraterrestrial solar irradiance: Providing a link between space-based and ground-based solar UV measurements, J. Geophys. Res., 106, D7, 7211–7217, 2001.

Gröbner J., Kouremeti, N. and Wehrli, C.: Atmospheric turbidity section (WRC-WORCC). PMOD/WRC Annual report 2014, available at: http://www.pmodwrc.ch/annual_report/2014_PMODWRC_Annual_Report.pdf, last access: 20 October 2016, 2015.

Gueymard, C.: SMARTS2, a Simple Model for the Atmospheric Radiative Transfer of Sunshine: Algorithms and performance assessment. Tech. Rep. FSEC-PF-270-95, 78 pp., available at:
rredc.nrel.gov/solar/models/smarts/relatedrefs/smarts2_report.pdf , last access 20 October 2016, 1995.

10 GUM: Evaluation of measurement data — Guide to the expression of uncertainty in measurement, Bureau International des Poids et Mesures, ISBN 92-67-10188-9, available at:
http://www.bipm.org/utils/common/documents/jcgm/JCGM_100_2008_E.pdf, last access: 20 October 2016, 2008.

Ingold, T., Mätzler, C., Wehrli, C., Heimo, A., Kämpfer, N., and Philipona, R.: Ozone column density determination from
15 direct irradiance measurements in the ultraviolet performed by a four-channel precision filter radiometer, Appl. Optics, 40(12), 1989–2003, 2001.

IPCC: Climate Change 2013: The physical science basis. Contribution of working group I to the fifth assessment report of the Intergovernmental Panel on Climate Change [Stocker, T.F., D. Qin, G.K. Plattner, M. Tignor, S.K. Allen, J. Boschung,
20 A. Nauels, Y. Xia, V. Bex and P.M. Midgley (eds.)]. Cambridge University Press, Cambridge, United Kingdom and New York, NY, USA, 1535 pp, doi:10.1017/CBO9781107415324, 2013.

Kasten, F. and Young, A.T.: Revised optical airmass tables and approximation formula, Appl. Optics 28, 4735–4738, 1989.

25 Kazadzis, S., Bais, A., Kouremeti, N., Gerasopoulos, E., Garane, K., Blumthaler, M., Schallhart, B., and Cede, A.: Direct spectral measurements with a Brewer spectroradiometer: Absolute calibration and aerosol optical depth retrieval, Appl. Optics., 44(9), 1681–1690, 2005.

Kazadzis, S., Bais, A., Amiridis, V., Balis, D., Meleti, C., Kouremeti, N., Zerefos, C. S., Rapsomanikis, S., Petrakakis, M.,
30 Kelesis, A., Tzoumaka, P., and Kelektsoglou, K.: Nine years of UV aerosol optical depth measurements at Thessaloniki, Greece, Atmos. Chem. Phys., 7, 2091–2101, doi:10.5194/acp-7-2091-2007, 2007.

Kerr, J., McElroy, C., Wardle, D., Olafson, R., and Evans, W.: The Automated Brewer spectrophotometer, in: Atmospheric Ozone, edited by: Zerefos, C. and Ghazi, A., 396–401, Springer Netherlands, doi:10.1007/978-94-009-5313-0, 1985.

Komhyr, W.D., Grass, R.D., and Leonard, R.K.: Dobson spectrophotometer 83: A standard for total ozone measurements, 1962-1987. J. Geophys. Res., 94, D7, 9847–9861, 1989.

Krotkov, N. A., Bhartia, P. K., Herman, J. R., Slusser, J., Labow, G., Scott, G., Janson, G., Eck, T.F., and Holben, B.: Aerosol ultraviolet absorption experiment (2002 to 2004), part 1: Ultraviolet multifilter rotating shadowband radiometer calibration and intercomparison with CIMEL sunphotometers, Opt. Eng., 44 (4), doi:10.1117/1.1886818, 2005.

Langley, S. P.: The "solar constant" and related problems, Astrophys. J., 17, 89–99, doi:10.1086/140999, 1903.

Li, Q., Li, C., and Mao, J.: Evaluation of atmospheric aerosol optical depth products at ultraviolet bands derived from MODIS products, Aerosol Science and Technology, 46:9, 1025–1034, DOI: 10.1080/02786826.2012.687475, 2012.

Marenco, F., Santacesaria, V., Bais, A. F., Balis, D., Di Sarra, A., Papayannis, A., and Zerefos, C. S.: Optical properties of tropospheric aerosols determined by lidar and spectrophotometric measurements (PAUR campaign), Appl. Optics, 36, 6875–6886, 1997.

Marenco, F., Di Sarra, A., and De Luisi, J.: Methodology for determining aerosol optical depth from Brewer 300–320 nm ozone measurements, Appl. Optics, 41, 1805–1814, 2002.

McPeters, R.D. and Labow, G.J.: Climatology 2011: An MLS and sonde derived ozone climatology for satellite retrieval algorithms, J. Geophysical Res., 117, D10303, doi:10.1029/2011JD017006, 2012.

Meeus, J.: Astronomical Algorithms, William Bell Inc., ISBN 0-943396-35-2, 1991.

Meleti C., Bais A.F., Kazadzis S., Kouremeti N., Garane K., Zerefos C.: Factors affecting solar UV irradiance, measured since 1990 at Thessaloniki, Greece, Int. J. Remote Sens., 30:15, 4167, 4179, 2009.

Michalsky, J. J.: The Astronomical Almanac's algorithm for approximate solar position (1950–2050), Solar Energy, 40(3), 227–235, 1988.

Mitchell, R. M. And Forgan, B. W.: Aerosol Measurement in the Australian Outback: Intercomparison of Sun Photometers, J. Atmos. Ocean. Tech., 20, 54–66, 2003.

Montenbruck, O. and Pfleger, T.: Astronomie mit dem Personal Computer, 2. Auflage, Springer, Berlin, ISBN 978-3-662-05860-2, 1994.

Nicolet, M.: On the molecular scattering in the terrestrial atmosphere: An empirical formula for its calculation in the homosphere. Planet. Space Sci., 32, 1467–1468, 1984.

Reda, I. and Andreas, A.: Solar Position Algorithm for Solar Radiation Applications. 55 pp.; NREL Report No. TP-560-34302, Revised January 2008, available at: http://rredc.nrel.gov/solar/codesandalgorithms/spa/, last access: 21 October 2016, 2003.

Redondas, A., Evans, R., Stuebi, R., Köhler, U., and Weber, M.: Evaluation of the use of five laboratory-determined ozone absorption cross sections in Brewer and Dobson retrieval algorithms, Atmos. Chem. Phys., 14, 1635-1648, doi:10.5194/acp-14-1635-2014, 2014.

Rieder, H. E., Holawe, F., Simic, S., Blumthaler, M., Krzyscin, J. W., Wagner, J. E., Schmalwieser, A. W., and Weihs, P.: Reconstruction of erythemal UV-doses for two stations in Austria: a comparison between alpine and urban regions, Atmos. Chem. Phys., 8, 6309–6323, doi:10.5194/acp-8-6309-2008, 2008.

Russell, P. B., Livingston, J. M., Dutton, E. G., Pueschel, R. F., Reagan, J. A., DeFoor, T. E., Box, M. A., Allen, D., Pilewskie, P., Herman, B. M., Kinne, S. A., and Hofmann, D. J.: Pinatubo and pre-Pinatubo optical-depth spectra: Mauna Loa Measurements, Comparisons, inferred particle size distributions, radiative effects and relationship to lidar data, J. Geophys. Res., 98, D12, 22969–22985, 1993.

Serdyuchenko, A., Gorshelev, V., Weber, M., and Burrows, J. P.: New broadband high-resolution ozone absorption cross-sections, Spectroscopy of Europe, 23(6), 14–17, 2011.

Shaw, G.E.: Sun photometry, B. Am. Meteorol. Soc., 64, 4-10, 1983.

Slusser, J., Gibson, J., Bigelow, D., Kolinski, D., Disterhoft, P., Lantz, K. and Beaubien, A.: Langley method of calibrating UV filter radiometers, J. Geophys. Res., 105, D4, 4841–4849, 2000.

Thomason, L. W., Herman, B. M., and Reagan, J. A.: The effect of atmospheric attenuators with structured vertical distributions on air mass determinations and Langley plot analyses, J. Atmos. Sci., 40, 1851–1854, 1983.

Tomasi, C., Vitale, V., Petkov, B., Lupi, A., and Cacciari, A.: Improved algorithm for calculations of Rayleigh-scattering optical depth in standard atmospheres, Appl. optics, 44(16), 3320–3341, 2005.

Vandaele, A. C., Simon, P. C., Guilmot, J. M., Carleer, M., and Colin, R.: SO_2 absorption cross section measurement in the UV using a Fourier transform spectrometer, J. Geophys. Res., 99, 25599–25605, 1994.

Weber, M., Gorshelev, V., and Serdyuchenko, A.: Uncertainty budgets of major ozone absorption cross sections used in UV remote sensing applications, Atmos. Meas. Tech., 9, 4459–4470, doi:10.5194/amt-9-4459-2016, 2016.

Wehrli, C.: Calibrations of filter radiometers for determination of atmospheric optical depth, *Metrologia*, 37, 419–422, 2000.

Wehrli, C.J.: Remote sensing of Aerosol Optical Depth in a Global surface network, Phd thesis, Diss. ETH No. 17591, ETH Zürich, Switzerland, 96 pp., available at: http://e-collection.library.ethz.ch/view/eth:30693, last access: 21 October 2016, 2008.

WMO/GAW: Experts workshop on Global Surface-based Network for long term observations of column aerosol optical properties, Davos, Switzerland, 8-10 March 2004. GAW report No. 162, WMO TD No. 1287, 153 pp., available at: http://www.wmo.int/pages/prog/arep/gaw/gaw-reports.html, last access: 21 October 2016, 2005.

WMO/GAW: Operations handbook – Ozone observations with a Dobson spectrophotometer revised 2008. GAW report No. 183, WMO TD No. 1469, 91 pp., available at: http://www.wmo.int/pages/prog/arep/gaw/gaw-reports.html, last access: 31 October 2016, 2009.

WMO/GAW: Eighth intercomparison campaign of the regional Brewer calibration center for Europe (RBCC-E), El Arenosillo sounding station, Huelva, Spain, 10-20 June 2013, GAW report 223, 79 pp, available at: http://www.wmo.int/pages/prog/arep/gaw/documents/FINAL_GAW_223.pdf, last access: 27 October 2016, 2015.

Table 1: Wavelength characteristics of UV-PFR#1001 based on laboratory measurements February 2016. The third column show effective central wavelength resulting from convolving the spectral response function with an extra-terrestrial solar spectrum.

Channel (nm)	Effective central wavelength (nm)	Convolved effective central wavelength (nm)	Bandwidth FWHM (nm)
305	305.35	305.31	0.99
311	311.36	311.34	1.04
318	317.55	317.50	1.20
332	332.33	332.32	1.26

Table 2: Langley calibration results for UV-PFR#1001 at Izaña 2015 and 2016, together with calculated V_0 and δ_o FWHM correction factors. Also the used Rayleigh optical depth and ozone absorption coefficients used for the UV-PFR#1001 are given.

Channel (nm)	Mean V_0 2015 (mV)	Std.dev. of V_0 (Std.dev of mean V_0) 2015 (%)	Mean V_0 2016 (mV)	V_0 change 2015–2016 (%)	FWHM correction factor for V0 c_{FWHM}	δ_o corr. factor at 350 DU, $\Delta\delta_{o,350DU}$	$\delta_{R,\lambda}$ Bodhaine (1999)	$k_{o,\lambda}$ B&P (-45°C) cm^{-1}
305	30319	1.28 (0.25)	30257	-0.2	1.012	-0.0045	1.1287	4.4682
311	11531	0.70 (0.13)	11522	-0.1	1.003	-0.0010	1.0377	2.0362
318	10669	0.82 (0.16)	10553	-1.1	1.001	-0.0004	0.9542	0.8802
332	5302	0.42 (0.08)	5248	-1.0	1.000	0	0.7856	0.0597
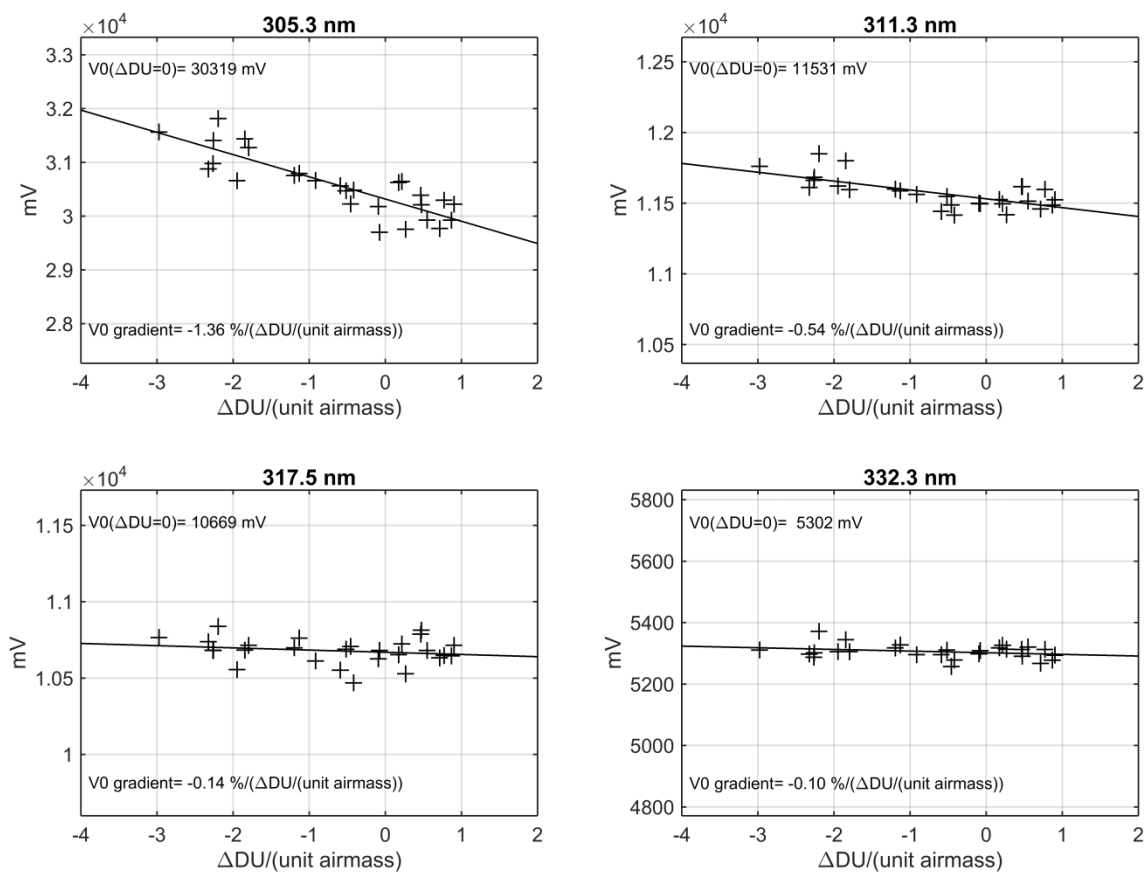
Figure 1: Results of all the Langley plot calibrations at IZO during May–August 2015. The final V_0s are derived from linear interpolation at zero ozone change. The ozone change during each Langley episode is calculated from linear fit of the Brewer triad total ozone values versus ozone airmass during the Langley event.
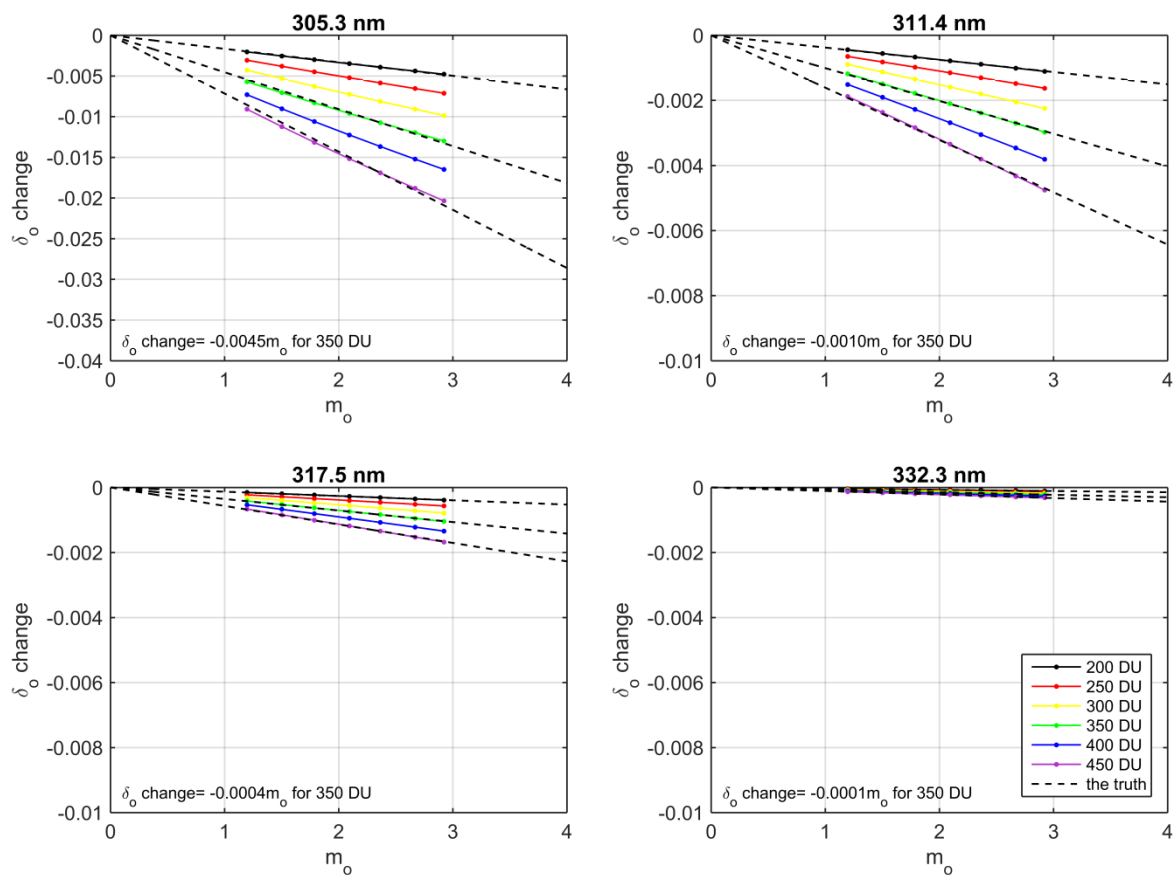
Figure 2: Calculated change in effective ozone optical depth with airmass due to the UVPFR filter bandwidths.
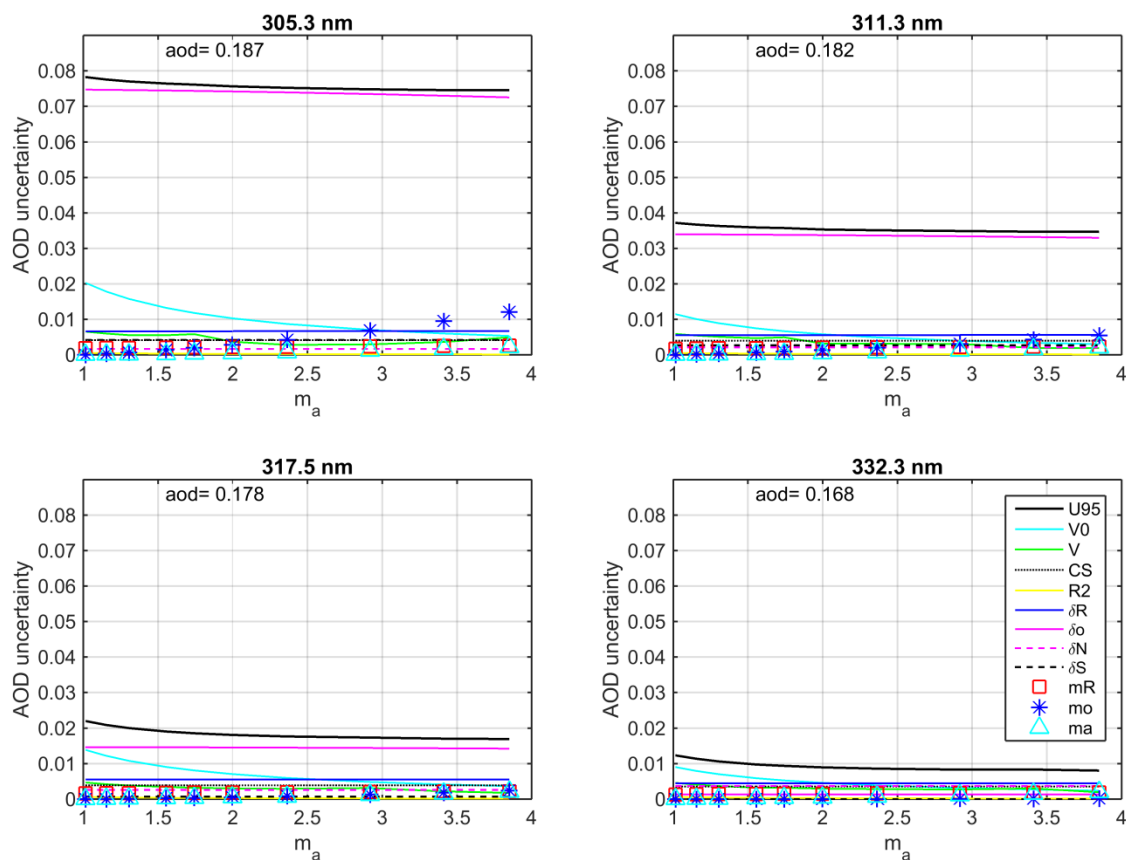
Figure 3: Estimated expanded uncertainties, k=2, (black lines) of AOD for the UVPFR #1001 wavelengths. Individual contributing uncertainties sources, at an approximate level of confidence of 95 %, are also shown. Calculations are made for a day 2 months after a calibration and with total column ozone amount of 350 DU.
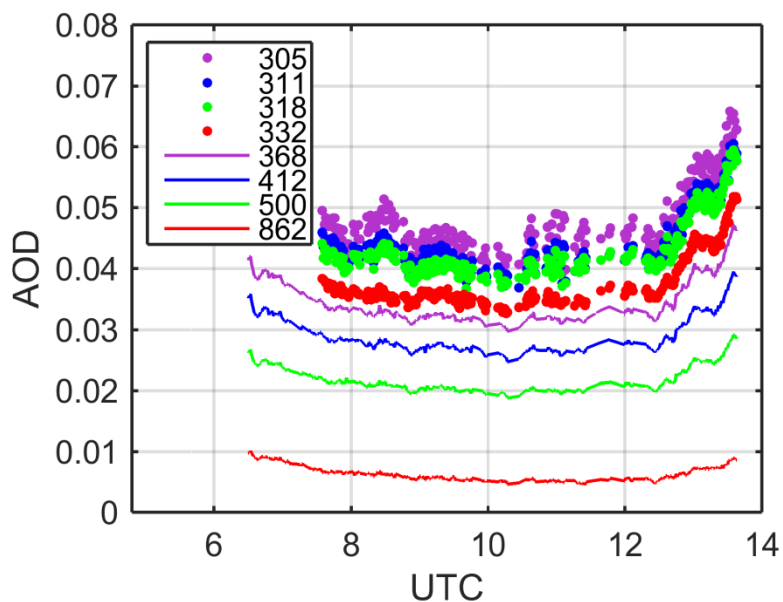
Figure 4: 1-minute AOD determined by UVPFR #1001 (dots) and PFR-N24 (lines) on the 12th October 2015 in Davos. Data points
5   **disturbed by clouds have been removed.**
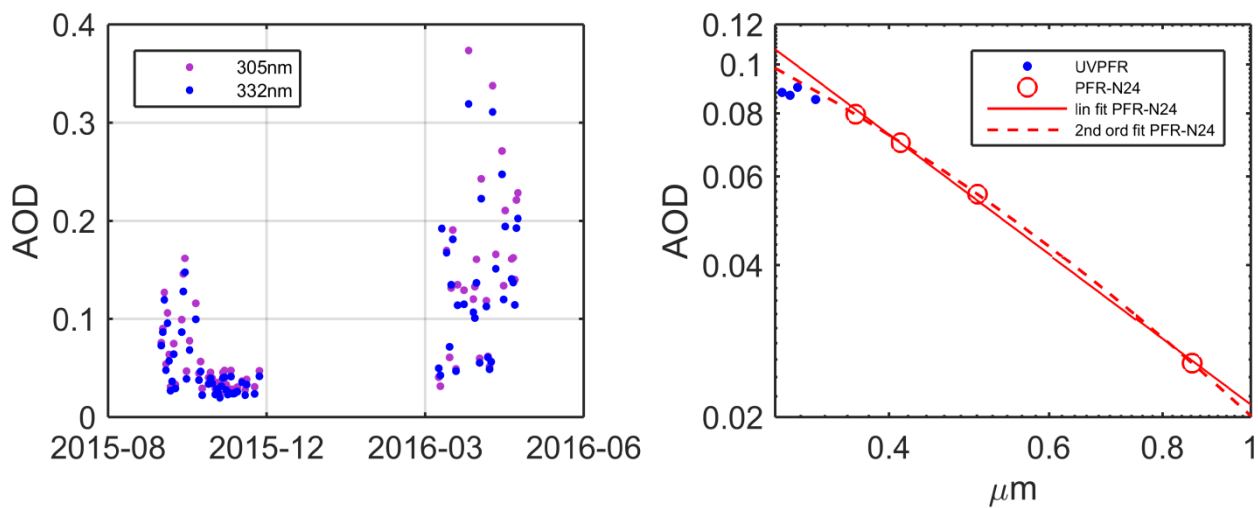
Figure 5: Daily mean AOD at 305 and 332 nm in Davos (left) and mean of daily means of AOD during the whole study from the
5   **UVPFR and a standard PFR (right).**
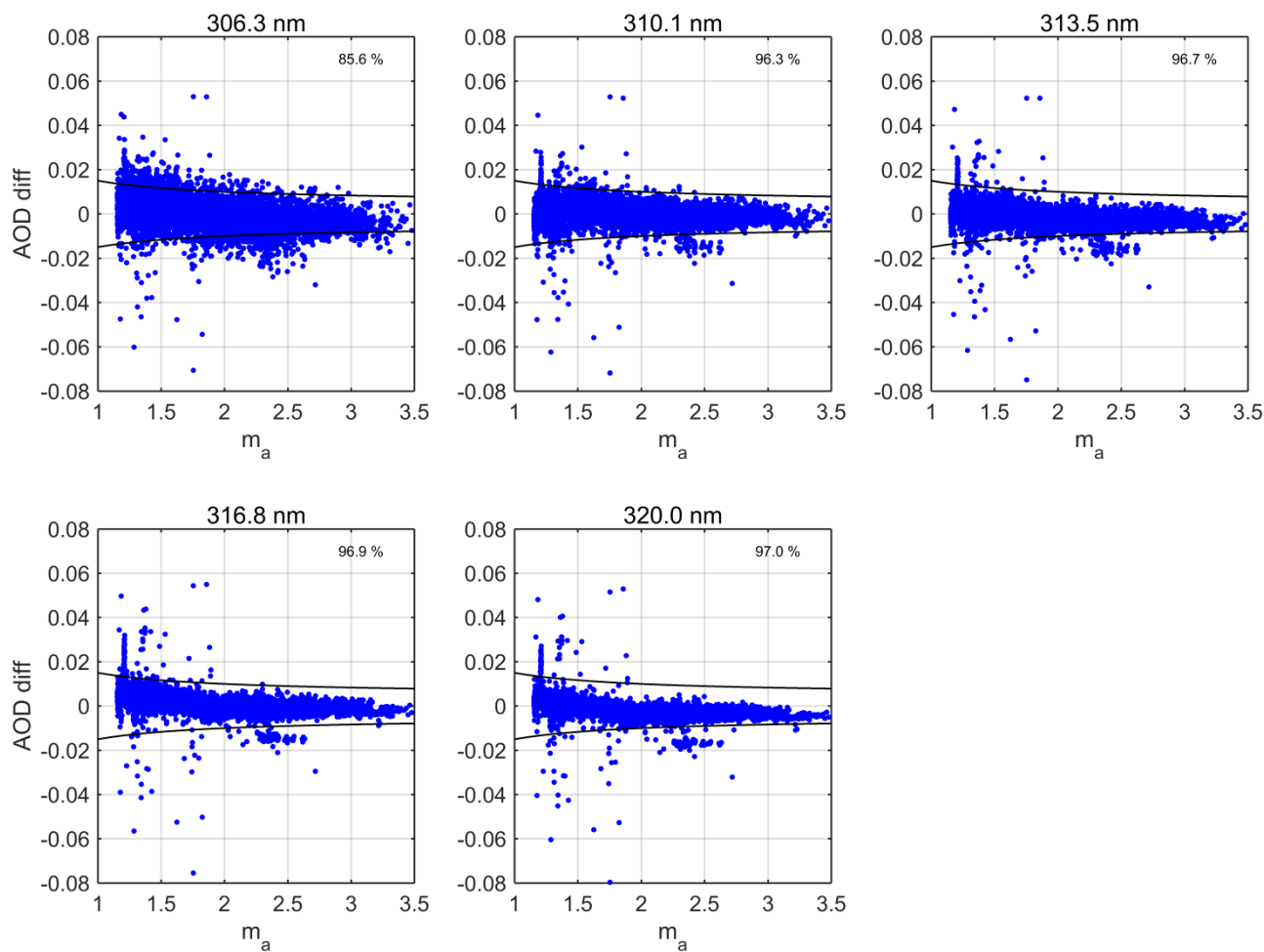
Figure 6: Differences in AOD, UVPFR-Brewer, at Brewer wavelengths for measurements during autumn 2015 and spring 2016 in Davos. Percentage of differences within WMO traceability limits is given in each graph.